doi.org/10.1002/hlca.202300223

RESEARCH ARTICLE

HELVETICA chimica acta

Development of a Novel Measurement Setup to Study and Predict Electrostatic Discharges in Agitated Glass-Lined Vessels

Benedikt Robert Brönnimann,[a] Daniel Egli-Tedesco,[b] Klaus Schwenzfeuer,[c] and Andreas Zogg*[a]

[a] University of Applied Sciences of Northwestern Switzerland, CH 4132 Muttenz, Switzerland,
e-mail: andreas.zogg@fhnw.ch
[b] Syngenta Crop Protection AG, CH-4058, Basel, Switzerland
[c] Hoffmann La Roche AG, CH-4070 Basel, Switzerland

Andrea Vasella gewidmet für seine Geistesblitze

Two glass lined reactors in a launch platform facility operated by Syngenta have been damaged during the crystallization of an organic compound due to electrostatic discharges. The goal of this work was to design and commission a novel setup to measure charges and currents generated by this slurry in a laboratory-scale reactor. An improved and more sophisticated setup was then proposed for possible implementation in Syngenta's own laboratories. With this novel setup, the electrostatic charging of stirred suspensions involving nonconductive solvents could be accurately measured in the context of a case study that involved the suspension that led to liner damages in the production facilities of Syngenta.

Keywords: Electrostatics, electrostatic charges, charge generation, electrostatic discharges, safety, stirred reactors, glass lined.

Introduction

Suspensions that contain a liquid-phase with low electric conductivity are prone to generate high electric charges when they are stirred and can produce powerful sparks when discharges occur. These sparks can penetrate protective coatings, such as enamel in glass lined equipment, and destroy them (*Figure 1*). Two 10 m^3 reactors were found to have sustained heavy damage after a crystallization had been performed in them. The characteristics of the found defects heavily imply strong electric discharges to be responsible. One of the reactors contained the liquid solution, consisting of an organic, dissolved compound and toluene at a concentration of roughly 30 wt% of solute. In this reactor, the mixture was cooled via cooling ramp and heavy stirring until the organic compound started to crystallize. This suspension was then transferred to the second reactor, which acted as a buffer tank.

Basics and Damage Mechanism

Liquids are electrostatically charged during flowing, stirring, and spraying. The level of charge increases with flow velocity, turbulence, and the size of the existing surfaces they move relative to, such as pipe walls, filter-meshes, etc..[1] The conductivity of a liquid has a dramatic effect on its charging ability. Liquids can be classified by their electric conductivity, high ($>$10000 pS/m), medium (50–10000 pS/m) and low ($<$50 pS/m).[2,3] Liquids with high conductivity can dissipate generated charge safely to earth by conducting it to the vessel or pipe wall. Fluids with medium conductivity can buildup critical charges, especially when said charge is generated rapidly. In such cases there may not be enough time to safely dissipate it to ground. Liquids with low conductivity are unable to dissipate static charge. Here, charge builds up even if the container is sufficiently earthed, hence it makes no difference if the container consists of an electrically conductible material or not. These liquids bear the highest risk in manufacturing processes.[4]

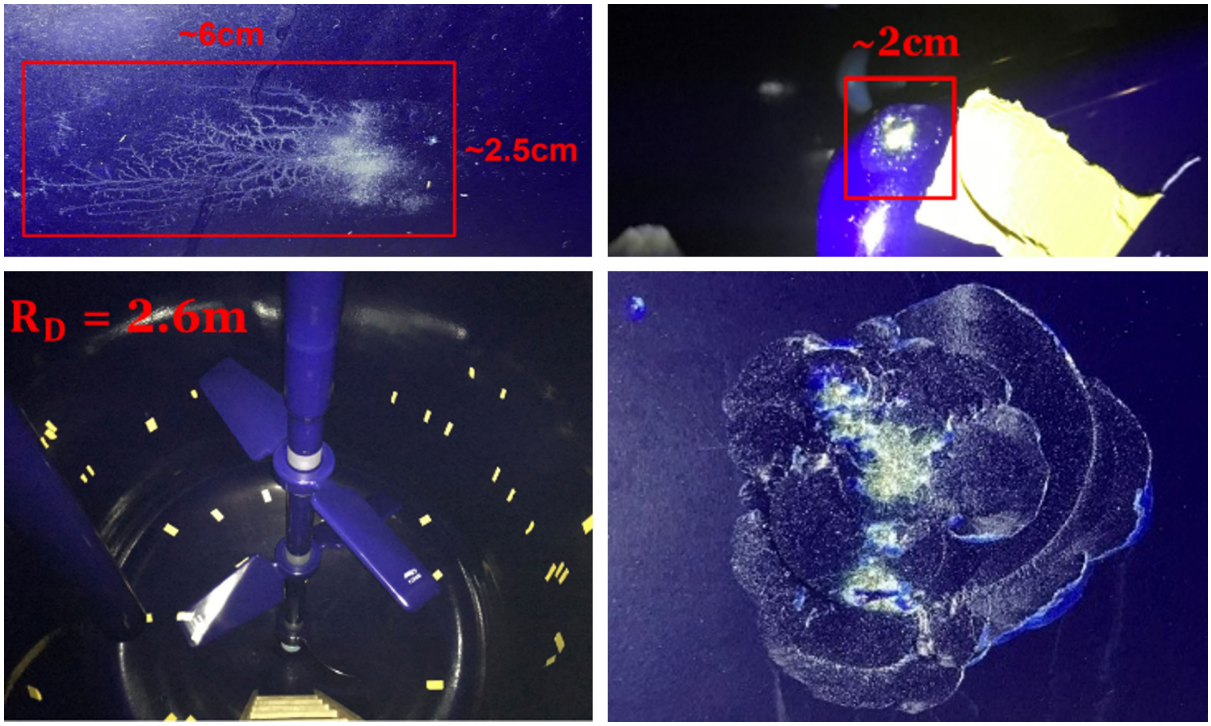

Figure 1. Some of the observed damages on the glass lined vessels.

Electrostatic discharges generally occur where the breakdown field strength of the surrounding medium is exceeded. Stirring liquids with low electric conductivity generate such high electric charges that brush discharges can be formed. These discharges are predominantly generated along the surface of the Liquid and spread out to the vessel wall, baffle, or stirrer. The part of the discharge with the highest energy will perforate the enamel at its weak point and produce a pore with reduced puncture resistance relative to its environment. Following discharges at the same location will further weaken the coating. Since these pores are often not visible by the naked eye, they can only be detected by means of spark testing or dying. If corrosive liquid penetrates the pore, the base material is attacked. The volume increase due to corrosion of the base material leads to flaking and the development of larger, noticeable holes. Large interfacial areas between the two phases in suspensions where electrical double layers can form on the particle surfaces are especially prone to electrostatic charging.[5]

Measuring Setup

As seen in *Figure 2*, the experimental setups main components are a glass-reactor, enclosed in a faraday-cage, all part of a scale down reactor, originally developed at FHNW for hydrogenation projects.[6,7] On the outside of the reactor, an electrically conductive layer (mantle electrode) was applied that allows the connection of a charge meter. The interior of the reactor contains several components, most notably the stirrer and an immersed electrode that is connected to an amperemeter. Alternatively, the immersed electrode may also be connected to a static voltmeter. The reactor contents could be tempered using a heating/cooling finger.[8,9]

Results and Discussion

Charges Measured with Mantle Electrode

In *Figure 3*, the total charges measured with the setup's charge meter are shown. They are presented in a three-dimensional manner with the stirring speed evident in the laboratory-reactor on its x-axis, the volume of the suspension on the y-axis and the maximal measured charge per experiment on the z-axis. The colored-in surfaces serve the purpose of improving the readability.

Throughout every experiment, the bulk of charge was produced shortly after the stirrer was turned on. After a few seconds of stirring the generation of charge started to slow down or halted completely. At the lowest

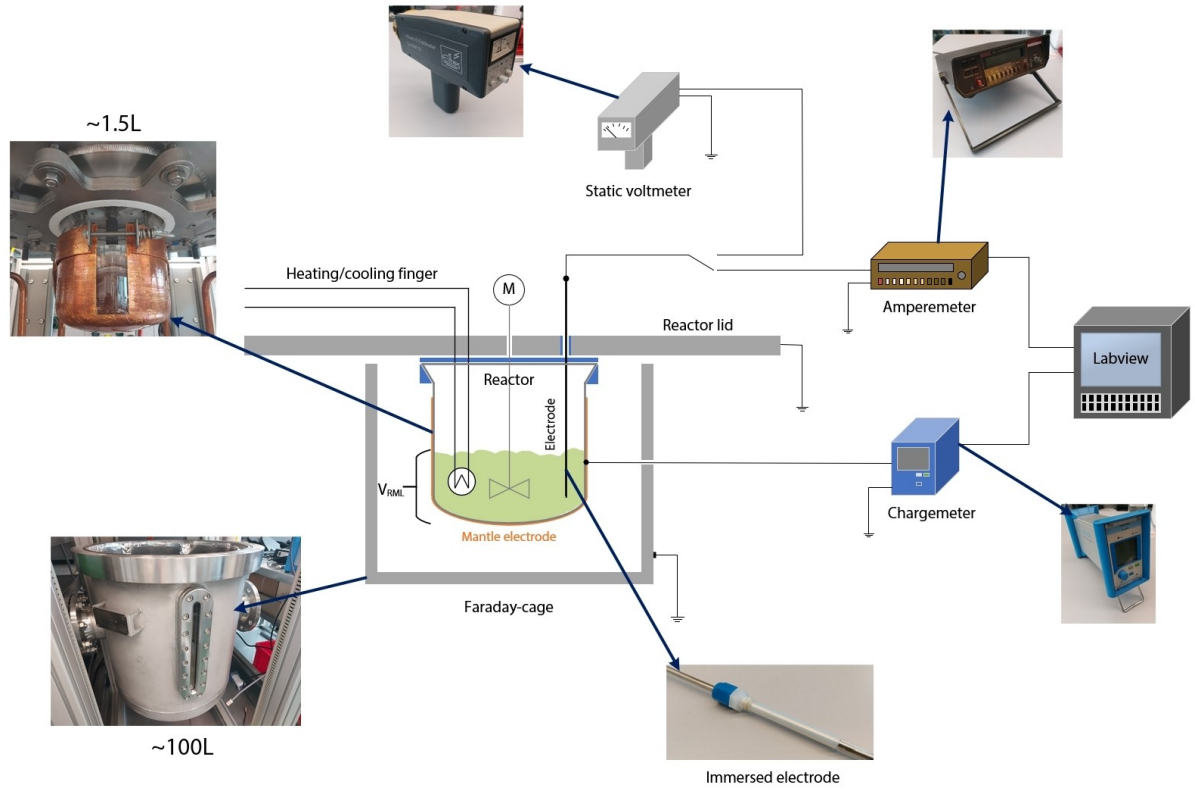

Figure 2. Schematic of the designed and commissioned experimental setup.

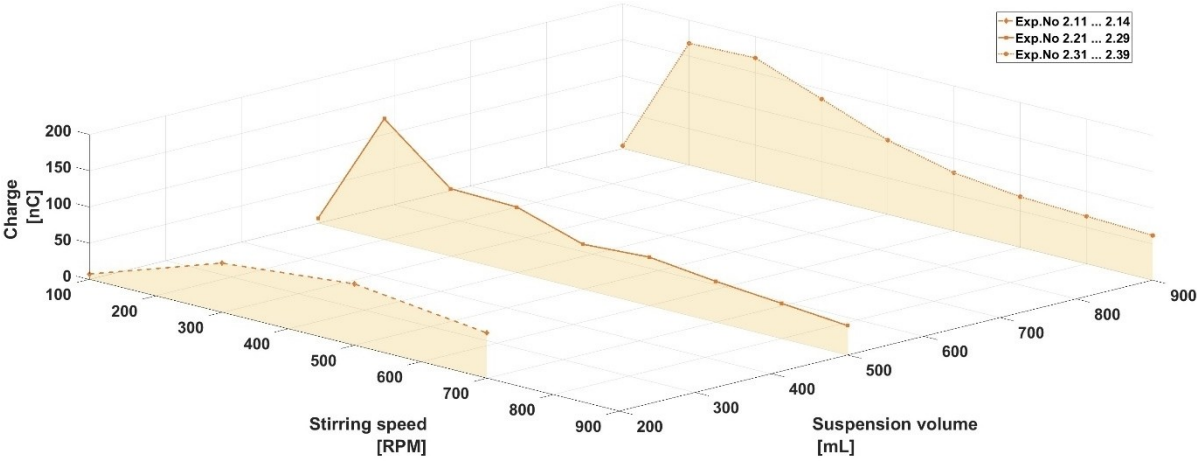

Figure 3. Maximum accumulated charges on mantle, plotted against various stirring speeds and suspension volumes (200; 500; 900 mL). The given experiment numbers are explained in more detail in *Table 1*. The suspension consists of toluene and the suspended organic compound (30 wt%), room temp: 20.3 °C.

suspension volumes, the charge even started to decrease while the stirrer was still in operation.

In *Figure 3*, it can be observed that at the lowest stirring speed (100 RPM) no charging was observed in any of the tested volumes. In general, lower speeds (200 … 300 RPM) generated the highest total charge. Further increases in agitator speed led to lower total charges. At the lowest volume, it was decided not to increase the agitating speed above 700 RPM, to avoid violent splashing and not put too much burden on the stirrer. For that same reason, fewer experiments were

performed in total for this volume. For better overview, the data is also presented in *Table 1*.

In *Figure 4*, the calculated currents I_M derived from the measured charge from the mantle-electrode are compared to the currents measured with the immersed electrode I_I.

I_M was determined by calculating the slope between adjacent elements in each of the executed experiments' charge-datasets. This effectively resulted in the rate of change over time, which is current. This differential data was then further analyzed by identifying the maximum calculated values. These peak current values I_M is what has been plotted in *Figure 4*. The median of the upper 10% of the currents measured with the immersed electrode for each experiment can be seen as well. The corresponding experiment numbers are also included.

Figure 4 shows that the measured currents of the electrode I_I were smaller than the calculated currents I_M derived from the measured charge of the reactor mantle. This is especially noticeable with a suspension volume of 900 mL. While total charges were higher at lower stirring speeds, the actual rate at which charge was generated remained lower compared to measured values at higher agitator speeds. This was also the case for the highest currents that were measured directly with the immersed electrode. Here, the highest currents always appeared immediately after the stirrer had been turned on, similar to what occurs on the mantle. At a certain point (600 RPM), an increase in speed did not result in higher generated currents.

In a next step, the volume specific current i_v could be calculated by dividing the measured maximum currents seen in *Figure 4* from the mantle-electrode I_I by the suspension volume present in the laboratory reactor V_{RML}. This then led to *Figure 5*. In this figure, the results in three separate runs of experiments. Each of the plotted lines correspond with a run of performed experiments at a suspension volume of 900 mL. Experiments 2.31 … 2.39 were performed with the charge meter still connected to the immersed electrode. For the latter experiments, a new batch of suspension was prepared, and the immersed electrode was either connected to a static voltmeter (No GP: Exp 2.51 … 2.59) or was connected directly to earth (GP: Exp 2.41 … 2.49).

Having the immersed electrode earthed or unearthed seemed to have no significant impact on the magnitude of the currents measured via the reactor mantle. Also, the first experiments (Exp 2.31 … 2.39) seemed to have

Table 1. Results of total charges measured on mantle as a function of stirring speed. All the results are given in nC.

Vol. [mL]	100 RPM	200 RPM	300 RPM	400 RPM	500 RPM	600 RPM	700 RPM	800 RPM	900 RPM
200	7.35		67.9		84.7		62.4		
500	6.7	167	93.3	90.7	62	67	56.4	48.6	40.5
900	3.8	167.8	170.4	136.5	102.4	80	69.7	65.6	61.9

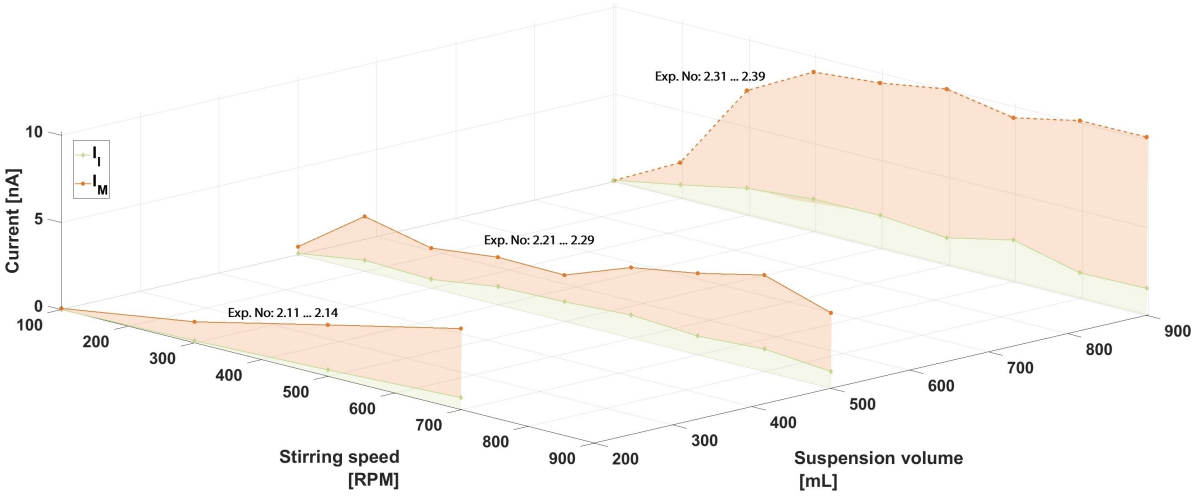

Figure 4. Comparison of measured currents Mantle-(I_M) and immersed-(I_I) Electrode current in relation to suspension volume and various stirring speeds with the corresponding experiment numbers. As mentioned, the currents shown here as I_M are derived from the measured charges from the charge meter. More information regarding how I_M is calculated, can be found in *Figure 8* and *Figure 9* of the experimental section.

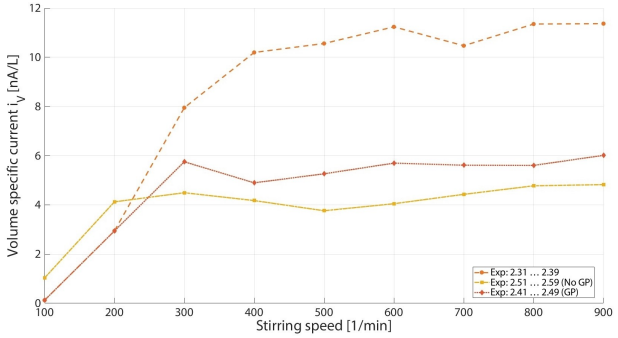

Figure 5. Calculated volume-specific current of the three separate runs with the suspension volume at 900 mL. The experiments marked GP (With grounding point) and No GP (No grounding point) were performed with a new batch of suspension.

yielded currents that are up to 100% higher than the currents measured in the repeated experiment with the newly mixed batch of suspension.

Comparable to *Figure 4*, higher currents correlated with higher stirring speeds, but started to reach saturation at 400 RPM. Responsible for this behavior are most likely the large crystals in the vessel. These crystals tended to remain in the bottom part of the reactor while the stirrer was in action, see *Figure 6*. At lower speeds, these crystals are only weakly swirled up and remain densely packed at the lower third of the reactor, while the lighter, smaller crystals are easily suspended throughout the total volume, even at slower stirring speeds. At lower speeds, these heavy crystals, although moving, only move in the bottom part of the reactor. Here, total **charges** were greatest (as seen in *Figure 3*). This gives reason to believe that the large crystals were responsible for the high charges because, while more densely packed, they can collide and separate again more frequently. At higher speeds, these large crystals are more evenly distributed throughout the suspension, and this seemed to lead to charges of smaller magnitudes.

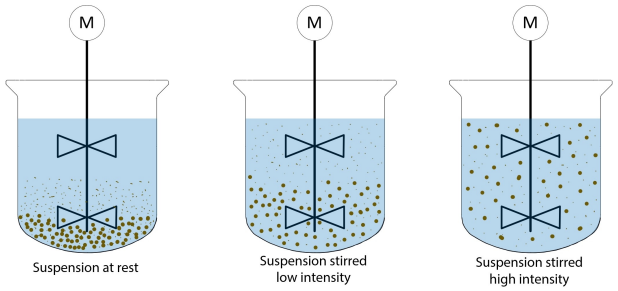

Figure 6. Observed suspension behavior under different stirring intensities.

The opposite could be observed with the measured currents, see *Figure 4* and *Figure 5*, which remained lower at low speeds and grew with an increase in agitator speed. This was most likely caused be the initial acceleration of the "crystal bed" when the stirrer was turned on. In every experiment, the rate of charge generated (and with that the calculated currents) was greatest in the first seconds of stirring, immediately after the agitator was activated. The generation of charge then significantly slowed or halted completely at high speeds when all the heavy crystals were more evenly distributed. The reason the volume specific currents from the first run shown in *Figure 5* are so different from the other two were most likely the inhomogeneities of the slurry batches. It could be possible that the second batch, used to perform experiments 2.51 … 2.59 and 2.41 … 2.49 contained less of the charge and current inducing large crystals than the batch that was used for experiments 2.31 … 2.39. Since it is suspected that the larger crystals are responsible for the high charging characteristics of the suspension, deviations of crystal concentration might have large influences on charging. This means, an absence of large crystals could lead to lower currents, while the presence of a larger amount would lead to higher charging.

Upscaled Discharge Energies

Both the theoretical discharge energies for the investigated suspension as well as pure toluene were calculated. For pure toluene, three measurements in total were performed. Compared to the discharge energies caused by the suspension, the energies produced by the batch of toluene were practically zero even at higher speeds (see blue dotted line in *Figure 7*).

An increase in stirring speed correlated with an increase in discharge energies. For easier comparison, the main x-axis shows the tip speed of the stirrer blades and the corresponding stirring speeds of the laboratory and production scale vessel. Production scale speeds ranged from 50 up to 90 RPM, whereas the laboratory stirrer could only "depict" speeds of up to ~67 RPM which corresponded to 900 RPM in the laboratory scale, its technical limit.

It can be observed that the charging of a slurry (straight line) and pure toluene (dotted line), is highly dependent on stirring speed, whereas the suspension is charged far more intense. Unfortunately, at the time this work was completed, there was no data available concerning the damage resistance of glass layers and the required energy to damage them.

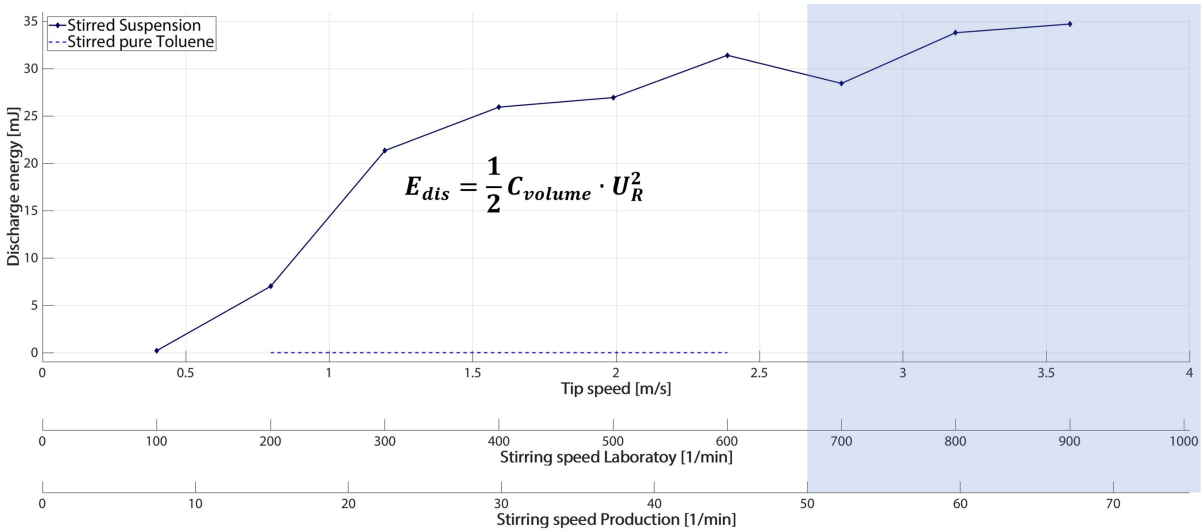

Figure 7. Theoretical, calculated discharge energies of a large production scale glass lined vessel with a working-volume $\mathbf{V_{RM}}$ of 5500 L and stirrer diameter of 1040 mm. The discharge energies $\boldsymbol{E_{dis}}$ [mJ] are calculated according to Eq. (12). Additional axes indicate the correlating stirring speeds in the production and laboratory scale reactor, correlated by tip speed. The stirring speeds evident at production scale when the damages took place are in the blue colored zone, and ranged from 50 and up to 90 RPM. The data from Exp. 2.31…2.39 were used for this comparison.

It is important to remark, that the calculations of the discharge energies were, in part, the result of several assumptions that were made which can have significant impact on said calculations. These include the resistivities of the glass layer and the suspension as well as the relative permittivity of the suspensionHere it was assumed that it was equal to the pure solvent, see Eq. (2), since the relative permittivity of the suspension itself could not be measured or determined in any other way while this work was being completed. The exact values which were used for the calculations are listed in *Table 2*.

Additionally, there are indications that the overall crystal composition of the investigated samples differed from the actual composition that was evident in the reactor during production, which in turn might have had great impact on charge generation while agitated. Unfortunately, due to time constraints, the impact that particle sizes and different solids have on charging behavior could not be thoroughly evaluated.

Furthermore, the geometries of the used instruments, such as stirrer, baffle, and the overall shape of the reactor-cup itself, were not like the instruments used in production on site. The experiments were performed at room temperature (~20 °C) not at 5 °C as was the case with the damaged reactors, since the setup's design did not allow for efficient cooling at the time this work was concluded.

Currently, qualitative differences, such as the impact of stirring speed and the charging behavior of slurries and pure solvents can be identified. There are clear and significant distinctions between the charging of pure solvent and suspension and a correlation between stirring intensity and discharge energy magnitude can be observed. The accuracy of the scale-up itself still needs to be determined.

Table 2. Necessary parameters and constants used for the calculations to obtain *Figure 7*. It is also shown for which equations the parameters were used.

Equation	Necessary parameters
Eq. (2)	Permittivity of free space: $\boldsymbol{\varepsilon_0} = 8.854 \cdot 10^{-12} \left[\frac{F}{m}\right]$
	Relative permittivity of dielectric: $\boldsymbol{\varepsilon_{Tol}} = 2.38$
Eq. (9)	Resistivity of suspension: $\boldsymbol{\rho_s} = 2.7 \cdot 10^{10}\ [Ohm \cdot m]$
	Resistivity of pure toluene: $\boldsymbol{\rho_{Tol}} = 1.7 \cdot 10^{12}\ [Ohm \cdot m]$
	Resistivity of glass-layer: $\boldsymbol{\rho_{En}} = 10^{13}\ [Ohm \cdot m]$

Conclusions

Setup

With the designed setup, currents and charges that are caused by electrostatic charging in an agitated glass vessel could be effectively measured.

Apart from being able to detect these small currents, charges and high voltages, their absolute values and the

general course of plotted data seem to have a systemic behavior that can be interpreted. *Figure 5* shows that, while there still are some disparities, a form of reproducibility between experiments and runs performed at the same filling level can be observed. Still, the total number of runs that were carried out remains small at this point. Ultimately, the calculated discharge energies, shown in *Figure 7*, are plausible from a relative point of view, but are small, with regards to their absolute values and further testing and experimenting is required.

Case Study

The observed results and the assumed behavior of the heavy crystals seen in *Figure 6* imply that at lower stirring speeds, these heavier crystals are contained at the reactor bottom and form a dense "cloud". In this cloud, these bigger crystals constantly encounter each other and are then separated again. Through this, electrostatic charge caused by charge separation is boosted which cannot dissipate because of the insulating nature of the used solvent.

At higher stirring speeds, the large crystals were lifted further and were distributed more evenly throughout the stirred suspensions volume. This led to less contact between large crystals throughout the investigated timeframes of stirring and, evidently, less total charge as seen in *Figure 3*. The highest currents I_M, however, were produced at higher speeds, mainly right after the stirrer had been activated. Here, the sedimented crystals are accelerated at a high rate. This rapid movement out of their resting position causes high rates of charge in short timespans. With that, high currents, and potentials are produced respectively. These values are significantly larger than what can be observed at low stirring speeds. After all the crystals have been lifted and dispersed into the suspensions volume, the charging rate is reduced significantly in contrast to lower speeds where the crystals remain low and dense which led to the large differences in total charge.

This was the case for two of the three suspension volumes (500 mL and 900 mL). At 200 mL, this phenomenon could not be observed in such a manner, most likely because the volume was too small. Repeating the process at 900 mL would further prove this assumption and show that a systematic phenomenon is at hands and a simple coincidence can be ruled out.

Overall, at this stage, it is possible to qualitatively describe this suspension regarding its charging behavior. From the electrostatic behavior of the system, it can be assumed that the size and quantity of the crystals might have had a substantial impact on the systems static up-charging. Although promising results have been obtained, the total amount of performed experiments is currently small and it is too early to draw any final conclusions regarding the magnitude of the calculated energies and if they are in realistic ranges.

Currently, these calculated discharges are, even though there is no referenceable data to compare to, unlikely to have enough energy to successfully damage enamel layers. The measured potential of the electrode on the experimental reactor was also low. This could have been the result of the used slurry which might not fully represent the suspension that caused the observed enamel damages in production. It now needs to be determined what crystal composition is present in the production scale reactors and characterize said slurry to then investigate it more accurately under more comparable and defined conditions in a laboratory environment, with more sophisticated instruments and an improved setup. Additionally, large scale experiments are essential to verify laboratory measurements and designed models. Tests with simple and easy to control systems could be a first step in this direction, such as saccharose as solid and again toluene as liquid.

Experimental Section

Setup to Measure Electrostatic Charges with the Mantle Electrode

To measure the generated charges inside of the reactor via mantle electrode, a charge meter was used. This device is capable of measuring charges with high accuracy and sampling rate. The charge meter itself was directly attached to the mantle's sleeve using a coaxial cable with two banana-plugs. The cable's shielding was grounded via direct connection to the reactor-lid. To ensure less interference, the distance between the two connected plugs (ground and signal) should be as small as possible. In *Figure 8*, the setup for charge-measurements is presented in a more detailed manner.

The high possible sampling rate of the charge meter of up to 200 kHz would have necessitated the used chassis and input module to process large amounts of data. For charge measurements, sampling rates of up to 100 Hz proved sufficient.

In *Figure 9*, a simplified view of the measurement process is shown. The charge-meter acquires a signal in the form of a charge dependent on time for each stirring experiment. This means that if the Exp. 2.31 … 2.39 are evaluated for example, a total of nine datasets are

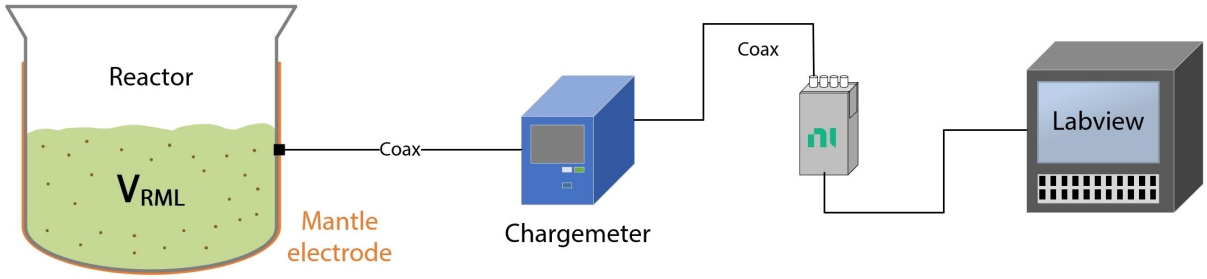

Figure 8. Diagram depicting the setup used to measure charge, with the glass-reactor wrapped in copper tape, acting as the mantle electrode.

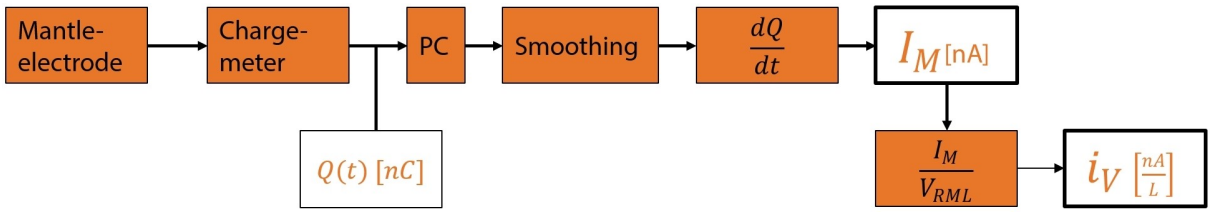

Figure 9. Block-diagram depicting a simplified view of data acquisition and signal processing method to determine $\mathbf{I_M}$ as well as $\mathbf{i_V}$ from the mantle electrode as seen in *Figure 4* and *Figure 5*.

available for evaluation. Each of these datasets are then smoothed using a moving average. After smoothing, the slope between adjacent elements from each dataset is evaluated (seen in *Figure 10* and *Figure 11*). The derivative of the steepest slope was then defined as the **mantle-current** $\boldsymbol{I_M}$/$_M$.

$$i_V = \frac{I_M}{V_{RML}} \tag{1}$$

Dividing the mantle current by the suspension volume $\boldsymbol{V_{RML}}$ according to Eq. (1) then led to the **volume-specific current** $\boldsymbol{i_V}$.

Setup to Measure Currents

To measure the generated currents, a metal electrode was fabricated and mounted to the reactor-lid. The electrode itself was cut from 6 mm stainless steel pipe. Its lower, later to be submerged end was welded shut. At its top, a latch was welded to the pipe for a banana-plug to be attached. A fitting was manufactured to fix the tube fitting and the inserted electrode to the lid. The tube fitting itself and the electrode's shielding were made from non-conductive polymers and were the most crucial part of the electrode since they ensured that no current could dissipate through the metallic reactor lid and could only flow via amperemeter, see *Figure 12*.

To directly measure the generated currents caused by stirring, an auto ranging picoammeter by Keithley was used. The device was then directly connected to the electrode via coaxial cable. The cable's shielding was also grounded by connecting it to the reactor-lid. Similar to the setup of the charge meter, the cable's shield plug and signal plug should be as close to each other as to reduce interferences.

Figure 12 depicts a diagram of the setup used to measure currents. The advanced age of the amperemeter made it necessary to connect it to the PC via IEEE-488 interface. While operating, the device was set in auto ranging mode.

In *Figure 13*, a simplified view of the measurement process is shown. The amperemeter directly detects currents caused by discharges onto the electrode. For evaluation, the top ten percent of measured currents at on specific stirring speed are evaluated. The median of these ten percent is then defined as $\boldsymbol{I_I}$, the **immersed electrode current**, this procedure is shown in more detail in *Figure 14*.

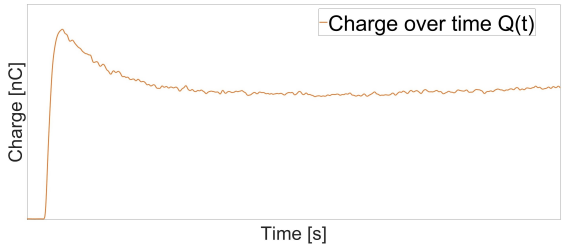

Figure 10. Example of smoothed charge measured over time in a single experiment.

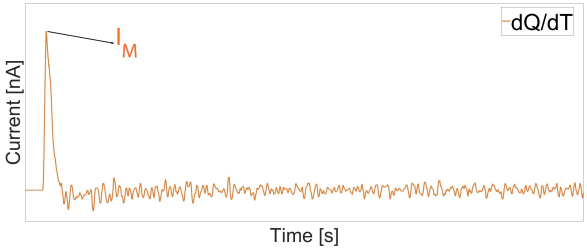

Figure 11. Resulting currents after evaluation. The highest current is defined as the mantle current for this experiment, which is then plotted in *Figure 4*.

Basic Principles of the Experimental Setup

Measured Volume of Immersed Electrode

Discharge energies generated were calculated under the assumption that the charge and discharge mechanism were comparable to that of a simple plate capacitor. Such a device can store electric charges, dependent on their capacity. The capacity C_{Volume} [F] of a plate capacitor is defined as follows in Eq. 2:

$$C_{Volume} = \varepsilon_{Tol} \cdot \varepsilon_0 \cdot \frac{A_C}{r_C} \tag{2}$$

With $\boldsymbol{\varepsilon_0}$ $\left[\frac{F}{m}\right]$ being permittivity of free space an $\boldsymbol{\varepsilon_{Tol}}$ $[-]$d the relative permittivity of the dielectric. It was assumed that this was equal to pure toluene. The area of the capacitor $\mathbf{A_C}$ [m^2] and the measured radius $\mathbf{r_C}$ [m] of the immersed electrode are explicitly shown in *Figure 15*.

To apply Eq. 2, the distance between the two capacitor plates $\mathbf{r_C}$ [m] needs to be determined first. *Figure 15* shows the most important parameters used to approximate the measured volume $\mathbf{V_I}$ [L] of the

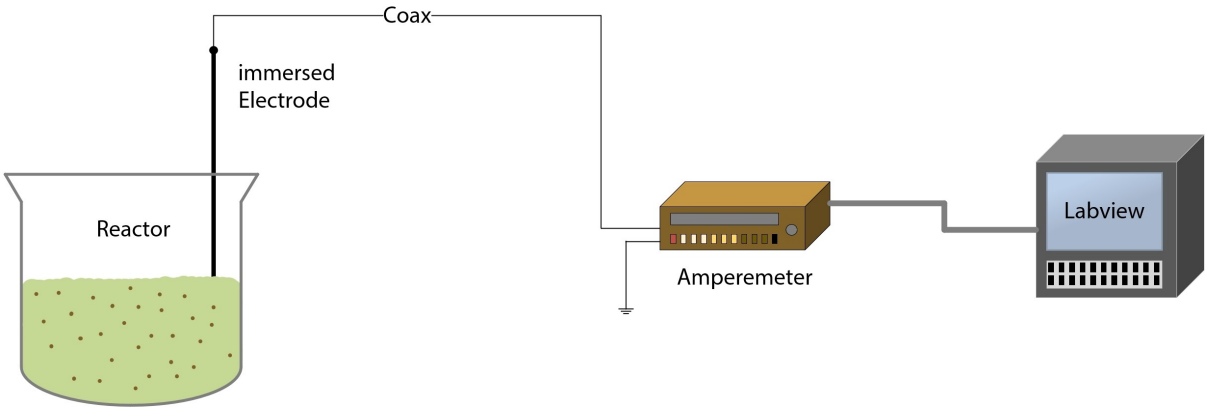

Figure 12. Diagram depicting the setup used to measure electrical currents.

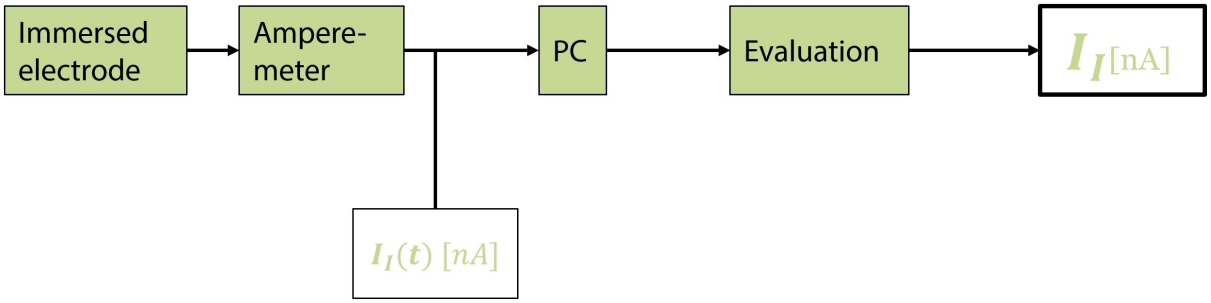

Figure 13. Block-diagram depicting a simplified view of data acquisition and signal processing to determine $\mathbf{I_I}$ from the immersed electrode as shown in *Figure 12*.

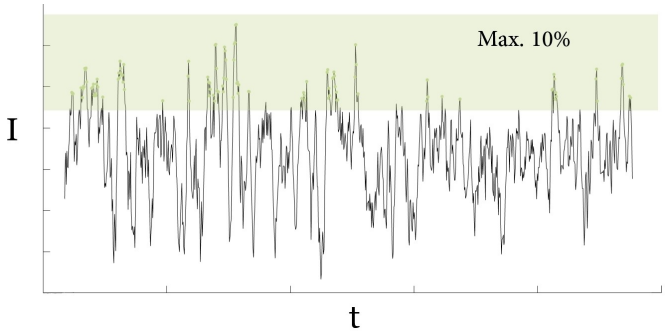

Figure 14. Example how the immersed electrode current was determined.

immersed electrode. Once the measurement volume has been determined, the diameter of the cylinder $\mathbf{D_{MI}}$ [m] can be calculated.

$\boldsymbol{V_I}$ [L] was determined by dividing the measured electrode current $\mathbf{I_I}$ [nA] by the volume specific current $\mathbf{i_V}$ [nA/L], obtained from the mantle electrode shown in *Figure 5*, using Eq. 3:

$$V_I = \frac{I_I}{i_V} \tag{3}$$

With the cylindric volume $\boldsymbol{V_I}$ now known and the depth of immersion $\mathbf{h_I}$ [m] and diameter of the electrode $\mathbf{D_{EL}}$ [m] also known, the total diameter of the cylindric volume element $\boldsymbol{D_{MI}}$ can be determined with Eq. 4 follows:

$$D_{MI} = 2\sqrt{\frac{V_I}{h_I}\pi} \tag{4}$$

These values are plotted in *Figure 16*.

We can see that, over the course of the conducted experiments, $\mathbf{D_{MI}}$ remained in realistic dimensions and started to become constant, even when stirring speeds were increased.

The cylinder is then projected onto a flat surface to obtain the desired cuboid volume element and its face plate surface $\mathbf{A_C}$, see Eq. 5. For the projection, the neutral phases of the cylinder were used, not the outer or inner diameters of the cylinder to ensure no stretching or compression of the surface takes place.

$$A_C = D_{IN} \cdot h_I \tag{5}$$

The "neutral diameter" $\boldsymbol{D_{IN}}$ of the cylinder can be determined using Eq. 6 as follows:

$$D_{IN} = \frac{D_{MI} + D_{EI}}{2} \tag{6}$$

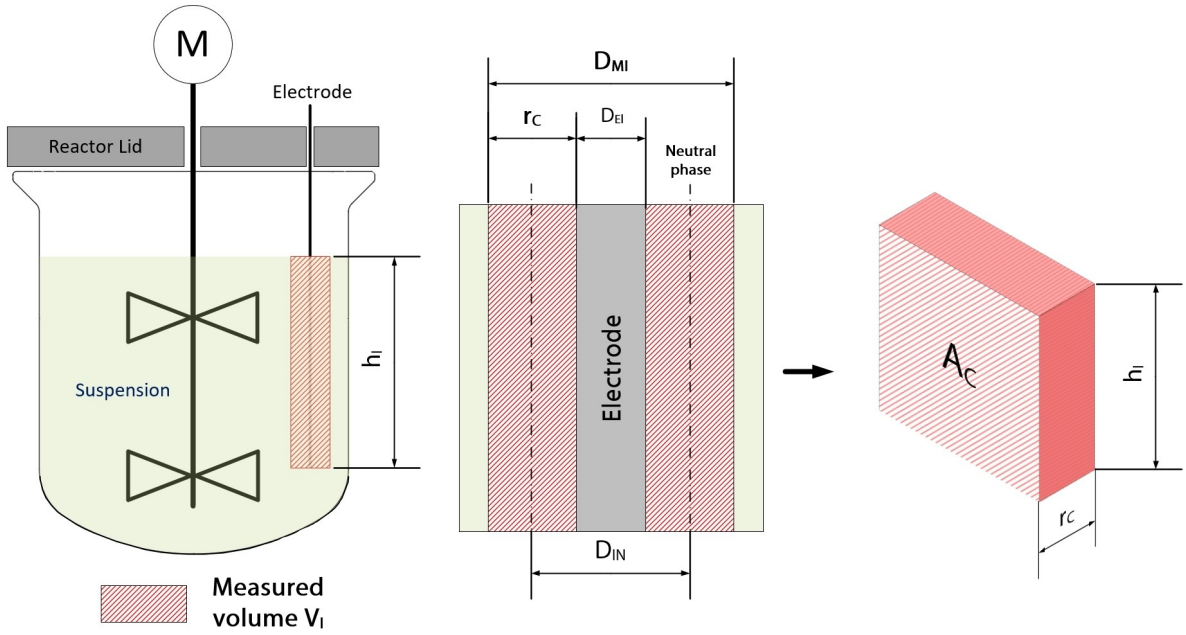

Figure 15. Measuring volume $\mathbf{V_I}$ [L]of immersed electrode with necessary parameters.

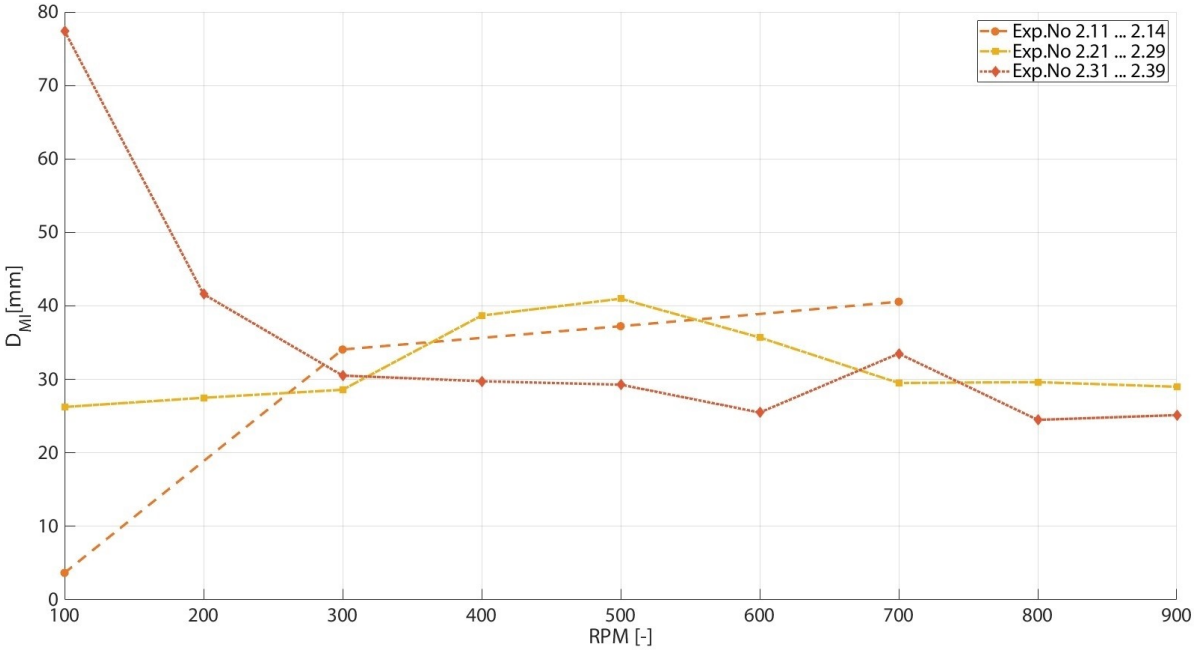

Figure 16. Calculated diameters of the cylindric volume element $\mathbf{D_{MI}}$ for each of the experiments at different stirring speeds.

Determining the Reactor Potential

At laboratory scale, it is feasible to measure the potential that is generated on the electrode using an electric field meter. It is also possible to calculate the resulting potential and scale it dependent on the size and volume of the investigated vessel. The potential can be calculated using the simple formula for Ohm's law, as shown in Eq. 7:

$$U_R = R_L \cdot I_{Rm} \tag{7}$$

Here, the potential $\mathbf{U_R}$ [V] is a result of multiplying the total earth leakage resistance of the vessel $\boldsymbol{R_L}$ [Ohm] with a current $\mathbf{I_{Rm}}$ [A]. This current can either be measured directly at the laboratory scale, or needs to be calculated with the following equation:

$$I_{Rm} = i_V \cdot V_{Rm} \tag{8}$$

The upscaled current $\mathbf{I_{Rm}}$ is, calculated according to Eq.8 by multiplying the volume specific current $\boldsymbol{i_V}$ [nA/L] and multiplying it with the total volume of suspension $\mathbf{V_{Rm}}$ [L] residing inside of the upscaled vessel (see *Figure 17*).

For the earth leakage resistance, Eq. 9 can be applied in case the investigated vessel is glass lined.

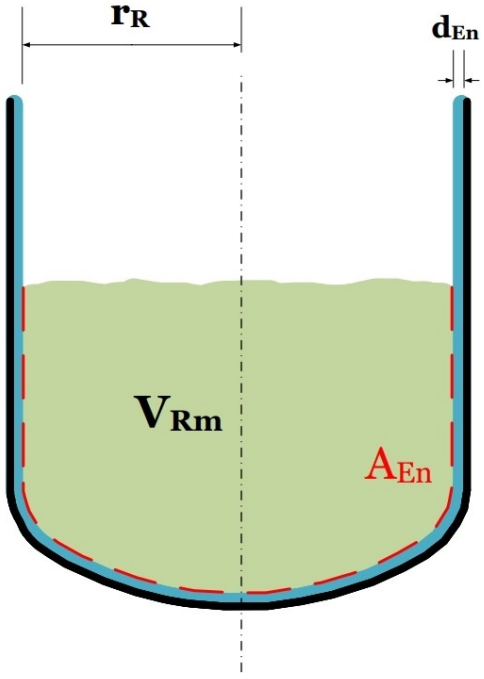

Figure 17. Simplified glass lined reactor model of a glass lined, production-scale vessel.

$$R_L = \rho_S \cdot \frac{r_R}{A_{En}} + \rho_{Em} \cdot \frac{d_{En}}{A_{En}} \tag{9}$$

With: $\boldsymbol{\rho_s}$ and $\boldsymbol{\rho_{En}}$ being the specific resistivities [Ohm·m] of the suspension and the glass-lining respec-

tively. As can be seen in *Figure 17*, $\mathbf{A_{En}}$ is the contact surface area of liner and suspension, and $\mathbf{d_{En}}$ is the thickness of the liner.

Discharge Energy

Charges inside of a medium may dissipate either via discharge or by charge relaxation.

A discharge between two materials is a rapid phenomenon and occurs when the breakdown field strength between two objects is exceeded.

The breakdown field strength in gases is dependent on several factors. In Air, it is mainly influenced by humidity and pressure.[10] In the case of air, the breakdown field at standard conditions is approximately 3MV/m.[11]

In contrast to other discharges, the discharge energy of spark discharges can be calculated from the voltage and the capacitance of the charged capacitor.

The discharge-energy of a capacitor can be described with the following equation Eq. 10:

$$E_{dis} = \frac{1}{2} \cdot \frac{Q^2}{C_{Volume}} \tag{10}$$

Here, E is the released Energy [J], Q is the amount of accumulated charge [C] and C_{Volume} is the capacitance of the system [F].

The Potential difference U [V] between two plates of a capacitor can be described as follows:

$$U = \frac{Q}{C_{Volume}} \tag{11}$$

Based on Eq. 11, Eq. 10 can be written as:

$$E_{dis} = \frac{1}{2} C_{volume} \cdot U_R^2 \tag{12}$$

This formula can later be utilized to determine the theoretical discharge energies in a production scale reactor. In this case, the equation with the filled in parameters looked at in the two previous sections is written as follows:

Overview of Performed Experiments

The following section contains *Tables 3*–5, whichlist all performed experiments. Each experiment of each run has been assigned a specific number to ease referencing.

Table 3. First run using toluene and solid at lowest fill level (25 %).

Exp. No	Mass solid [g]	Mass Toluene [g]	Solid weight fraction [wt %]	Stirrer Speed [RPM]	Reactor Temp. [°C]	Room Temp. [°C]	Rel. Humidity [%]
2.11	59.4	138.7	30	100	20.3	20.3	33
2.12	59.4	138.7	30	300	20.3	20.3	33
2.13	59.4	138.7	30	500	20.3	20.3	33
2.14	59.4	138.7	30	700	20.4	20.3	29

Table 4. Second run.

Exp. No	Mass Solid [g]	Mass Toluene [g]	Solid weight fraction [wt %]	Stirrer Speed [RPM]	Reactor Temp. [°C]	Room Temp. [°C]	Rel. Humidity [%]
2.21	148.5	346.5	30	100	21.12	19.1	42
2.22	148.5	346.5	30	200	21.12	19.1	42
2.23	148.5	346.5	30	300	21.12	19.1	42
2.24	148.5	346.5	30	400	21.12	19.1	42
2.25	148.5	346.5	30	500	21.12	19.1	42
2.26	148.5	346.5	30	600	21.12	19.1	42
2.27	148.5	346.5	30	700	21.12	19.1	42
2.28	148.5	346.5	30	800	21.12	19.1	42
2.29	148.5	346.5	30	900	21.12	19.1	42

Table 5. Third run.

Exp. No	Mass Solid [g]	Mass Toluene [g]	Solid weight fraction [wt%]	Stirrer Speed [RPM]	Reactor Temp. [°C]	Room Temp. [°C]	Rel. Humidity [%]
2.31	326.7	762.3	30	100	20.2	20.3	40
2.32	326.7	762.3	30	200	20.2	20.3	40
2.33	326.7	762.3	30	300	20.2	20.3	40
2.34	326.7	762.3	30	400	20.2	20.3	40
2.35	326.7	762.3	30	500	20.2	20.3	40
2.36	326.7	762.3	30	600	20.2	20.3	40
2.37	326.7	762.3	30	700	21.17	19.2	38
2.38	326.7	762.3	30	800	21.17	19.2	38
2.39	326.7	762.3	30	900	21.17	19.2	38

Author Contribution Statement

B.R.B. developed and installed the setup, performed all experiments, analyzed the data, and penned and finalized the manuscript. K.S. contributed knowhow and the basic idea on how to calculate discharge energies. He also performed resistance measurements of the investigated slurry. D.T and A.Z. acted as expert and supervisor respectively, and provided resources and premises for the experiments and overlooked the project in general. All authors commented on the manuscript.

Acknowledgements

The Authors would like to acknowledge the support of Peter Steigmeier, who has contributed great effort and important equipment to complete this work. B.R.B would also like to thank the team at Syngenta for the opportunity to work at their facilities infrastructure and resources, especially Marc Neff who originally set this work in motion. Open Access funding provided by Fachhochschule Nordwestschweiz FHNW.

Data Availability Statement

The data that support the findings of this study are available from the corresponding author upon reasonable request.

References

[1] G. Lüttgens, W. Schubert, S. Lüttgens, U. von Pidoll, S. Emde, *Statische Elektrizität: durchschauen - kontrollieren - einsetzen*, Wiley-VCH, Weinheim, 2020.
[2] L. G. Britton, *Avoiding Static Ignition Hazards in Chemical Operations*, Center for Chemical Process Safety of the American Institute of Chemical Engineers, New York, 1999.
[3] 'Technische Regeln für Gefahrstoffe 727' 2016.
[4] M. R. Giles, 'Electrostatic Hazards in Liquids and Relevance to Process Chemistry', *Org. Process Res. Dev.* **2003**, *7*, 1048–1050.
[5] B. Maurer, 'Damage to enamel on stirred apparatus triggered by static electricity discharges of material being stirred', *J. Electrost.* **1997**, *40–41*, 517–522.
[6] T. Furrer, B. Müller, C. Hasler, B. Berger, M. K. Levis, A. Zogg, 'New Scale-Up Technologies for Hydrogenation Reactions in Multipurpose Pharmaceutical Production Plants', *Chimia* **2021**, *75*, 948–948.
[7] T. Furrer, M. Levis, B. Berger, M. Kandziora, A. Zogg, 'New Scale-Up Technologies for Multipurpose Pharmaceutical Production Plants: Use Case of a Heterogeneous Hydrogenation Process', *Org. Process Res. Dev.* **2023**, *27*, 1365–1376.
[8] J. Asprion, A. Zogg, 'Die Chemie Pilotanlage der FHNW Muttenz' **2023**, DOI 10.26041/FHNW-4990
[9] 'Homepage Miniplant 4.0', can be found under https://www.fhnw.ch/plattformen/miniplant40/, n.d.
[10] B. Ritz, 'Durchschlagfeldstärke des homogenen Feldes in Luft.' **n.d.**, 14.
[11] M. Glor, P. Turnherr, Schweizerisches Institut zur Förderung der Sicherheit, 'Zündgefahren durch elektrostatische Aufladungen in der Prozessindustrie' 2016.

Received December 8, 2023
Accepted January 18, 2024

